

E-VTOL Concept Design with a New Underwing ‘FanFoil’ Ducted Fan Concept to Improve Aerodynamic Efficiency

Jack Hicks and Victor Maldonado*†*

**Texas Tech University, Lubbock, TX 79409, USA*

jack.hicks@ttu.edu – victor.maldonado@ttu.edu

† Corresponding Author

Abstract

This paper proposes a novel transitioning eVTOL aircraft concept utilizing distributed underwing ducted fans with a specially designed undercambered airfoil presented as the ‘Maldonado-Hicks’ airfoil. It is hypothesized that this concept where the airfoil is blended into the fan on the aft portion of the airfoil, referred to as the ‘FanFoil’ concept, is aerodynamically superior to mounting the fans over the wing. This is due to the ability to recess and partially hide the fans underneath the wing, such that the fans are not entirely visible in forward flight when looking at the wing from the front. It is expected that this ‘FanFoil’ technique reduces the form drag of the wing with distributed fans. In this initial study, computational fluid dynamic (CFD) simulations are performed on the Maldonado-Hicks airfoil which represent a two-dimensional section of the eVTOL wing at the cruise conditions; Mach 0.22 (260 km/h) and Reynolds number of 6.5×10^6 . The lift and drag coefficients are computed in order to get an understanding of the cruise angle of attack and design lift coefficient that maximizes aerodynamic efficiency as quantified by the lift-to-drag ratio, L/D . Open vehicle sketch pad (VSP) is also used to perform a low-fidelity CFD analysis of the clean eVTOL configuration. The base drag coefficient, C_{D0} is estimated as 0.018. Finally, an idealized steady-state analytical mission analysis is completed for a hypothetical maximum-range mission for a 5-passenger eVTOL concept. Based on power and energy consumption calculations, it is estimated that this aircraft concept attains a maximum range of 290 km with a 300 kW-h size lithium polymer battery and a usable energy of 270 kW-h.

1. Introduction

Electric vertical takeoff and landing concepts or e-VTOLs for point-to-point passenger flight in congested cities have emerged due to the maturation of key technology, particularly efficient, high power density electric motors coupled with safe lithium polymer batteries with increasing energy densities. A variety of e-VTOL configurations have been proposed, each with perceived mission and operational advantages [1]. In general, these vehicles offer safety, reliability, efficiency, with low noise compared to conventional forms of air travel [2]. There are several e-VTOL aircraft in the fledgling Advanced Air Mobility (AAM) market that are currently undergoing flight testing and certification. Two leading examples of such aircraft developed by Joby Aviation and Archer Aviation employ a distributed propeller or open rotor propulsion architecture [3, 4]. Large propellers that operate at lower speeds offer a higher ‘figure of merit’ or aerodynamic efficiency with lower noise compared to ducted fans or propellers which are significantly smaller and must operate at high speed. However, aircraft with distributed ducted fans are deemed safer for passengers (due to ducting the fan) and mitigate the unsteady flow and aerodynamic interaction between the ducted fan jet and aircraft wing/body. This decrease aerodynamic interference and form factor to produce an aircraft with generally higher cruise lift-to-drag ratio, L/D . The Lilium jet is a rare example of an eVTOL that uses distributed ducted fan propulsion [5]. A total of 36 ducted fan propulsors (24 on the main wing and 12 on the canard wing) are mounted on top of the wing on the flap surface which rotates to enable flight transition. An added advantage to ducted fans when mounted next to a surface is

DOI: ADD DOINUMBER HERE

that the inflow ingests the developing boundary layer, thereby reducing the viscous drag generated over that surface.

Boundary layer ingestion (BLI), a concept under research by the National Aeronautics and Space Administration (NASA) since 2019, is a process in which the boundary layer flow along the surfaces of an aircraft is ingested along with the freestream airflow by the aircraft's propulsion system. Research from NASA's Glenn Research Center indicates a potential performance increase of up to 8.5 percent compared to non BLI systems [6]. In BLI propulsion, the duct or nacelle of a propulsion system is blended into either the lifting surface or fuselage surface of an aircraft. This causes the boundary layer airflow along the craft's surface to be ingested by the propulsion system's intake. This flow, which is normally associated with surface drag in traditional aircraft designs, is accelerated by the craft's propulsion system, adding energy into the flow and reducing surface, wake, and jet dissipation. These dissipation reductions reduce drag across the aircraft's mission so that less energy input is required to obtain the same thrust as traditional propulsion systems [7]. Incorporating BLI into an aircraft design can result in increased flight efficiency and mission endurance, which is advantageous for an eVTOL aircraft as it provides the necessary improvements to reduce battery energy needs. In the last few years, Maldonado's research group has been active in the conceptual design of unique aircraft concepts. In particular, a robotic ground-aerial vehicle for Mars planetary exploration [8], a four-variant reconfigurable flying wing unmanned aerial vehicle (UAV) for commercial applications [9], and a two-variant multi-flight regime reconfigurable combat aerial vehicle [10]. This paper explores the conceptual design of an eVTOL utilizing distributed ducted fan propulsion. However, rather than placing the ducted fans above the wing, they are mounted underneath the wing in the aft region of the airfoil. A specially designed airfoil, introduced for the first time in this study as the 'Maldonado-Hicks' airfoil, was created to serve two unique purposes: (1) partially hide the ducted fans when looking at the aircraft from the front, thereby reducing the frontal cross-section wing area and its expected form drag, and (2) serve as a pre-inlet for the fans by gradually expanding the flow and reducing inflow distortion into the duct inlet and fan. An initial computational study of the Maldonado-Hicks airfoil in isolation and applied to an eVTOL concept is investigated. The integration or blending of the airfoil with the ducted fan is referred to as the 'FanFoil' concept.

2. FanFoil Concept

2.1 Maldonado-Hicks Airfoil

The 'Maldonado-Hicks' airfoil family is a set of highly undercambered airfoils designed for the use of underwing distributed ducted fans for propulsion. The airfoils operate with a slight negative angle of attack, allowing the ducted fan mounted in the aft region to be partially hidden from front view. It is hypothesized that the wing form factor, F and form drag is reduced in this configuration, compared to where ducted fans have their entire frontal cross section area exposed to the flow. Both the upper and lower surfaces (denoted by subscripts u and l) of the airfoil are defined by coordinates, z/c from continuous 5th order polynomial functions of the form below with a dimensionless chord distance, x/c ,

$$(z/c)_{u,l} = a(x/c)^5 + b(x/c)^4 + c(x/c)^3 + d(x/c)^2 + e(x/c) \quad (1)$$

The functions are subject to the following boundary conditions at the trailing edge, $x/c = 1.0$ and at the fan inlet, $x/c = 0.60$ respectively,

$$\frac{dy_u}{dx} = -\frac{dy_l}{dx} \quad (2)$$

$$\frac{dy_l}{dx} = 0 \quad (3)$$

The smooth curvature also allows the pressure surface to act as a pre-inlet diffuser for the duct, reducing flow distortion into the inlet and fan interface. At an angle of attack, α of zero, the polynomial function was parameterized to produce a slope of zero at a dimensionless chord distance, $x/c = 0.6$ (boundary condition), which is where the inlet of the ducted fan should be placed. In order to study the aerodynamic characteristics of the airfoil implemented on the wing of the eVTOL, a specific airfoil was created with a camber of 7% and a thickness of 10% based on chord.

2.2 ANSYS Setup and Analysis

Computational fluid dynamics (CFD) simulations using ANSYS Fluent was utilized to predict the aerodynamic lift and drag coefficients of the Maldonado-Hicks airfoil at a Reynolds number of 6.5×10^6 and Mach number of 0.22. These flow parameters represent the cruise conditions of the mean aerodynamic wing chord for the concept eVTOL design

presented later in this paper. The geometry of the fluid domain for the analysis of the airfoil consists of a 6m by 4m boundary with a half-circle end with a radius of 2m. The airfoil tip is located on the center point of the half-circle and acts as an interior wall within the fluid domain. Additional area was included behind the airfoil to capture turbulence and disturbances in the flow pattern caused by the wing. Figure 1 shows the geometry of the fluid domain around the airfoil. The average element size used across the fluid domain was 250mm with smaller element sizes present closer to the airfoil surface. The mesh used in the evaluation of the Maldonado-Hicks airfoil chosen for the eVTOL design may be seen in Figure 1. The fluid domain mesh consisted of 4621 nodes and 4433 elements. A refinement level was applied along the airfoil surface to improve the accuracy of the airfoil analysis. The SST K-Omega turbulence model was used to simulate the flow over the airfoil. The inlet conditions include a flow velocity in the X-direction of 70 m/s. The outlet conditions were kept at zero gauge pressure. The walls and airfoil were simulated as non-slip wall conditions.

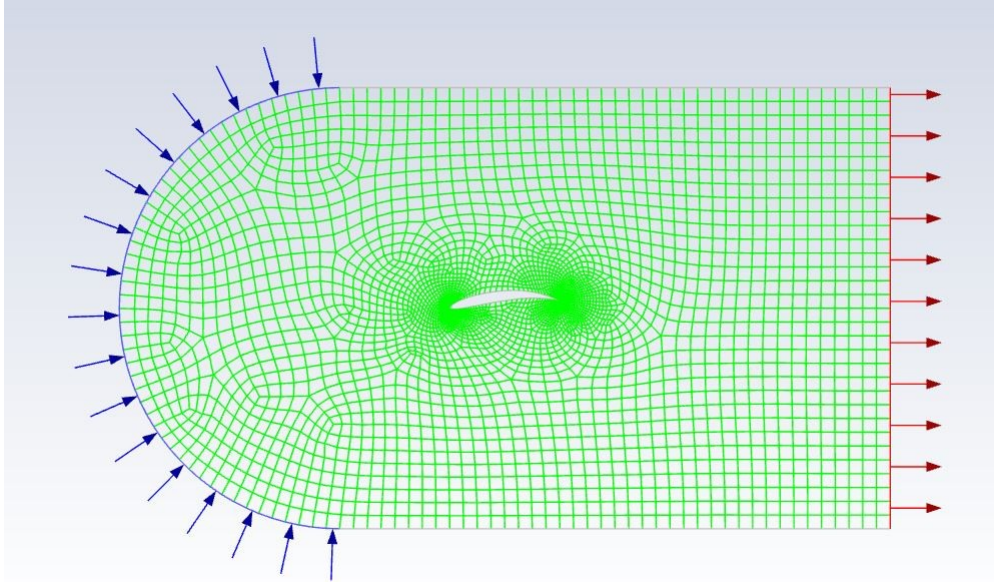


Figure 1: Airfoil fluid domain and mesh setup

The preliminary CFD analysis was carried out in order to obtain an understanding for the values of lift coefficient produced at certain angles of attack, and if the airfoil would operate efficiently (with sufficiently high L/D) at low negative cruise angles of attack. Based on the analytical design lift coefficient calculated, $C_{L,d} \approx 0.45$ for the fixed-wing eVTOL concept, and correction to the 2D airfoil design lift coefficient, $C_{L,d}$ of 0.70, it was determined that the eVTOL concept would cruise at a negative angle of attack, $\alpha_{cr} = -4$ degrees. Figure 2 is a pressure contour plot of the Maldonado-Hicks airfoil representing the mean aerodynamic chord of the wing for the cruise conditions of the eVTOL concept.

Simulations of the lift and drag coefficients of the airfoil for angles of attack between -15 to 20 degrees were also conducted and plotted on Figures 3 to 5. Results show a fairly linear lift-curve-slope, $C_{L,\alpha}$ with a value of 0.10/deg which is fairly typical for 2D airfoil flows. The drag polar behavior is predictable and indicates the airfoil achieves a base drag coefficient, C_{d0} of 0.013 for a small range of angles in the drag bucket from -5 to -2 degrees, which includes the cruise angle of attack. Finally, the plot of the L/D ratio on Figure 4 indicates that the airfoil in cruise ($\alpha = -4$ deg) operates with $L/D = 47$ which is considerably far from the optimum L/D peak of 60 at approximately $\alpha = 4$ deg. Additional simulations with small design variations of the Maldonado-Hicks airfoil are being processed in order to fine-tune the aerodynamic characteristics and shift the L/D peak to a negative angle of attack. Furthermore, it is important to note that even though the L/D peak may be lower compared to conventional airfoils (e.g., NACA 4-digit series), its negative angle cruise orientation allows a ducted fan to be mounted underneath the airfoil while minimizing additional form drag compared to an airfoil with a fully exposed fan.

DOI: ADD DOINUMBER HERE

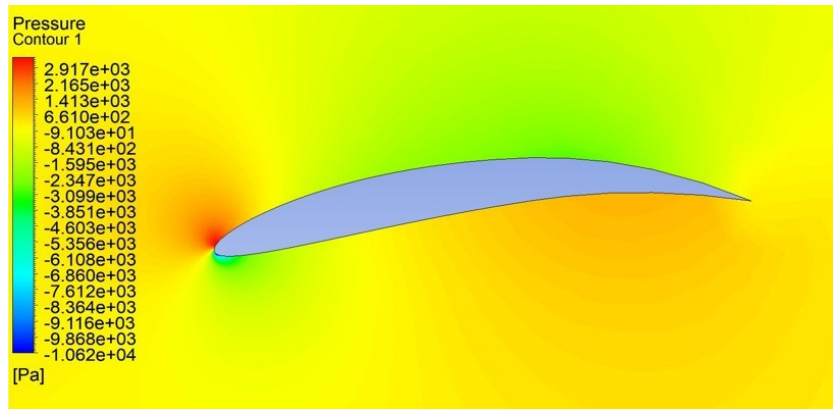


Figure 2: Maldonado-Hicks airfoil pressure contour representing the wing mean aerodynamic chord and the cruise flow conditions ($Re_c = 6.5 \times 10^6$ and $M_C = 0.22$) for the eVTOL concept.

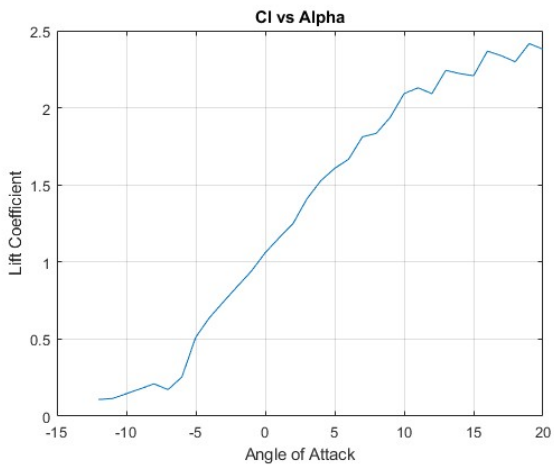


Figure 3: Lift coefficient, C_l vs angle of attack, α

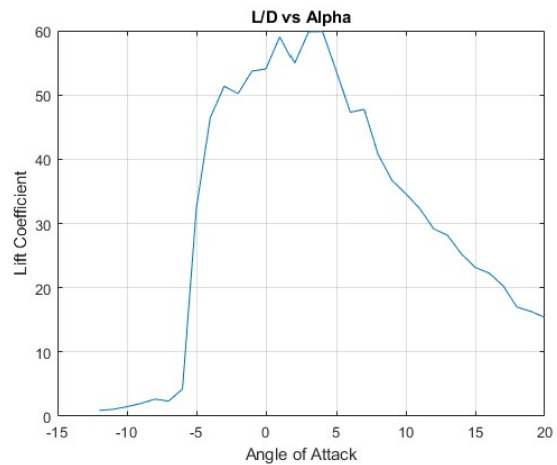


Figure 4: Lift-to-drag ratio, L/D vs angle of attack, α

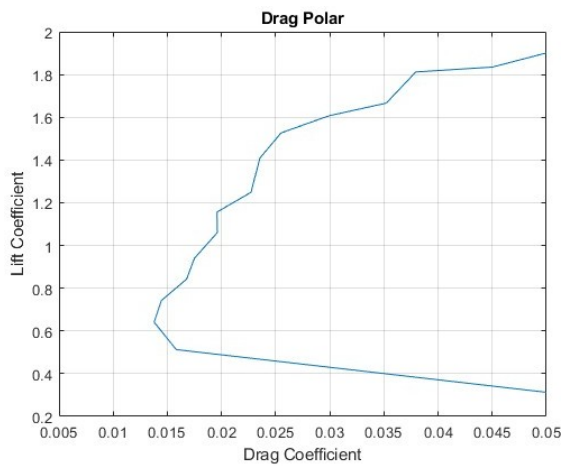


Figure 5: Drag polar, C_d vs C_l

DOI: ADD DOINUMBER HERE

2.3 Underwing Mounted Ducted Fans

The concept of the ‘FanFoil’ is to integrate the ducted fan in a manner where the main wing airfoil and the ducted fan located in the aft region of the airfoil are blended as one assembly. This configuration offers certain aerodynamic advantages: (i) partially hide the ducted fan reducing the frontal profile area of the wing thus reducing its aerodynamic form factor and drag, (ii) the underside of the airfoil acts as a diffusing pre-inlet for the fan reducing flow distortion on the rotor plane, and (iii) the boundary layer developed on the underside of the airfoil is ingested by the fan inflow thereby minimizing viscous drag. The FanFoil concept is illustrated on Figure 6, where Fig. 6a) is the main wing geometry for the eVTOL concept partially showing the fans in the aft region of the wing, Fig. 6b) is a side profile of the airfoil and a ducted fan array, and Fig 6c) is a front profile of the wing showing that the ducted fans are partially hidden underneath the main wing and theoretically contribute to a reduction in the form factor and total drag of the wing. Note that the concept design is a work-in-progress, and the duct is not yet fully blended as the trailing edge region of the airfoil which will become a flap structure with distributed fans that can rotate in order to achieve thrust vectoring and flight transition on the eVTOL concept. An initial concept for the flap (which will become the rear 40% section of the airfoil) with ducted fans is illustrated on Figure 7. Note the ducted rotors contain rotor blades designed with elliptical planforms inspired from the maple seed. This blade shape is expected to improve the lift-per-unit span distribution and downwash to improve aerodynamic efficiency and mitigate acoustic noise from vortex shedding at the blade tip.

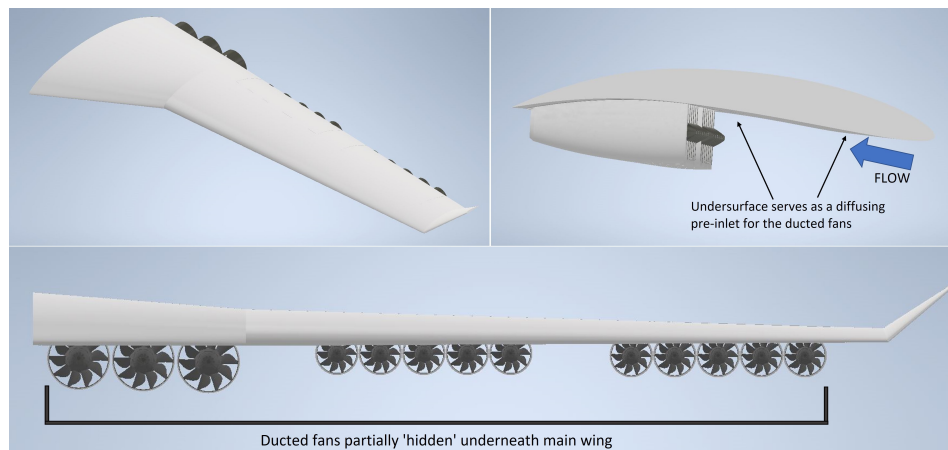


Figure 6: FanFoil concept a) Main wing geometry, b) Side profile showing Maldonado-Hicks airfoil in aircraft cruise orientation with undersurface acting as a diffusing pre-inlet for the ducted fans, and c) front profile showing ducted fans partially hidden underneath main wing to reduce the wing form factor.

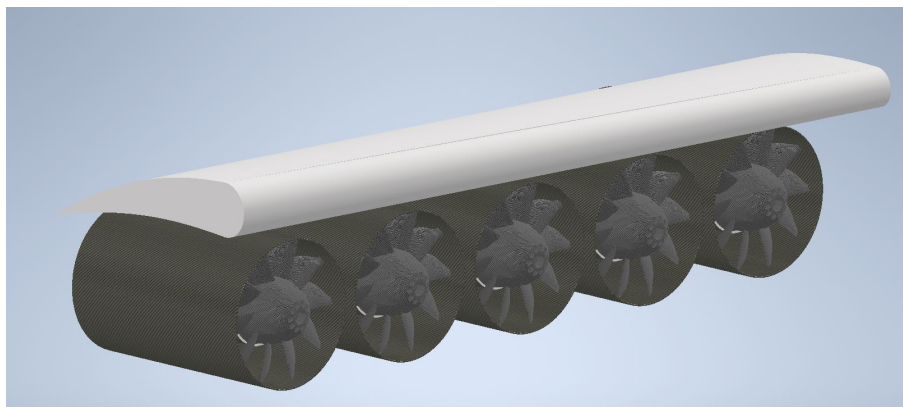


Figure 7: Ducted fan flap section: initial modeling to integrate onto the main wing and allow thrust vectoring for flight transition.

3. eVTOL FanFoil Aircraft Conceptual Design

The eVTOL concept with the integrated FanFoil technology is unique in the growing Urban Air Mobility industry. A render of the eVTOL conceptual design depicting takeoff or landing from a grass field is shown on Figure 8. The vast majority of concepts and prototypes being tested contain open rotors with complex vortical flow-fields that interact with the body and wing of the aircraft. This scenario produces more spanwise and unsteady separated flow conditions over parts of the lifting wing surface and body, leading to ‘dirty’ aerodynamics that reduce the overall aerodynamic efficiency or L/D in forward flight. In contrast for this proposed eVTOL design, the jet-like flow-fields produced by the ducted fans are isolated underneath the wing, leaving the flow over the wing surface largely unaffected, thus improving the lift-per-unit span, L' and aerodynamic efficiency of the wing.

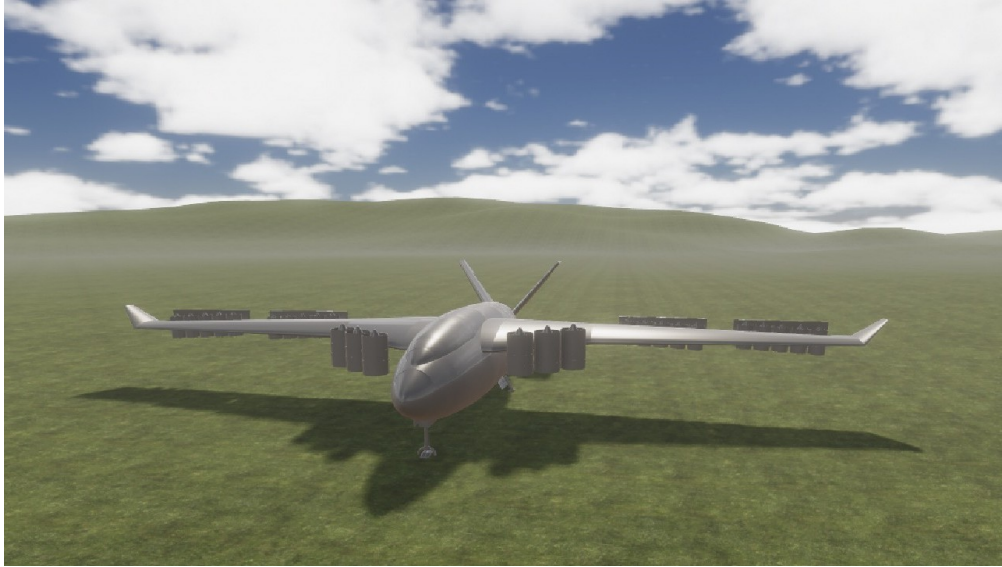


Figure 8: eVTOL conceptual design with ducted fans in vertical takeoff and landing configuration

3.1 Conceptual Design Features

The eVTOL concept was designed using first-order analytical formulation contained in the literature, e.g. [11, 12]. Some aspects of the conceptual design process are discussed while omitting the formulation for brevity. The unique features of the aircraft are also described along with the main design variables and specifications.

1. Initial Sizing

The aircraft was conceived as a 4-5 passenger aircraft that can use existing technology to achieve its mission of transporting passengers a minimum distance of 241 km, which is considered practical. Next, the cruise speed of the aircraft was set at Mach 0.22 which is 260 km/h at the cruise altitude of 2,439 m (8,000 ft) above sea level. A battery energy and specific energy density that reflects the size of battery this concept might use for its mission was selected. A battery capacity of 300 kW-h and energy density of 320 W-h/kg is specified. However, only 90% of the battery energy is usable, or 270 kW-h, to avoid over-discharging which can be harmful. Based on these values, a battery mass of 938 kg is found. The takeoff weight of the eVTOL is estimated by considering 5 people and light luggage as a payload, which factors in 100 kg each or 500 kg total. A structure factor, s of 0.40 reflecting a modern light but strong composite structure is applied, which is defined as the eVTOL empty weight (not including payload or battery) divided by the takeoff weight. We can now estimate the takeoff weight as 2,400 kg. A summary of the mission flight requirements and static loads are stated on Table 1.

Table 1: Mission requirements and load variables

Mission Requirements	Mission Value	Load Variables	Load Value
Minimum range, R	241 km	Battery mass, m_B	938 kg
Cruise Mach, M_c and speed, V_∞	0.22 (260 km/h)	Payload	500 kg
Cruise altitude, H	2,438 m	Structure factor, s	0.40
		Takeoff weight, W_{T0}	2,400 kg

2. Configuration

The eVTOL configuration is a high-wing aircraft with a V-tail and dual control surfaces to accomplish flight stability and control. There are a total of 26 ducted fans mounted on the wing; six large fans (rated at 140 kW power each) on the inboard wing panels, and 20 regular ducted fans (rated at 75 kW each) mounted on four flaps on the outer wing panels. During flight transition from VTOL to forward flight, the large fans move using a hydraulic system from the leading edge of the wing (as picture on Fig. 8) to the trailing edge for forward flight. In the process, thrust is vectored from hover to forward flight as is required. In a similar fashion, the ducted fans on the wing flaps rotate with an angular range of 90 degrees for thrust vectoring during flight transition. During flight, roll moments and control is achieved using the outer flaps which effectively become active ailerons with ducted fans. Modeling the flight transition of the eVTOL and control of the ducted fans is beyond the scope of this study.

The fuselage design was lofted using Sears-Haack functions where an exponent parameter, p was tuned in order to shape the gradient of the curvature for the curves that define the fuselage boundaries. The dimensions of the fuselage, particularly length, L , maximum width, w , and maximum height, h , were fixed to satisfy volume requirements and accommodate the pilot and passengers, the lithium-polymer battery, and other required internal hardware, avionics and components. The V-tail was sized according to design formulation, where the tail planform area, S_{VT} is a function of wing span, b wing planform area, S_W , and the axial distance between the V-tail and wing. The airfoil selected for the tail surfaces is a NACA 0010 airfoil which is adequate for increased aerodynamic lift and control authority for low subsonic flight aircraft. A summary of the main aircraft design variables are given on Table 2.

Table 2: Wing, fuselage, and V-tail design variables

	Wing	V-tail	Fuselage
Airfoil	Maldonado-Hicks	NACA 0010	
Planform area, S	21.79 m ²	4.11 m ²	
Span, b	14.49 m (with winglets)	2.72 m	
Aspect ratio, A	9.63	3.60	
Leading edge sweep, Λ_{LE}	35° and 5°	20°	
Taper ratio, λ	0.34	0.60	
V-tail separation angle, Γ		80°	
Length, l			8.72 m
Maximum width, w			1.85 m
Maximum height, h			1.78 m
Fineness ratio, d_{max}/l			0.21

4. Open VSP Model and Analysis

4.1 Computational Model

DOI: ADD DOINUMBER HERE

The eVTOL concept was modeled using Open Vehicle Sketch Pad. OpenVSP was created by NASA for a streamlined approach to 3D modeling and low-fidelity CFD analysis for aerospace applications. Specific design variables were calculated using design formulation first and then implemented into OpenVSP. For the wing modeling, the software provides the ability to import Cartesian coordinate plots in .dat format including airfoil coordinates for the Maldonado-Hicks airfoil. The fuselage was defined using Sears-Haack functions and implemented on OpenVSP using import settings such as manual tracing and sectioning. Sectioning is where the user divides the fuselage shape into many parts and modifies its dimensions to meet the desired shape. The V-tail was modeled using the same method as the wings. A 3D model of the baseline eVTOL concept without the ducted fans is illustrated on Figure 9.

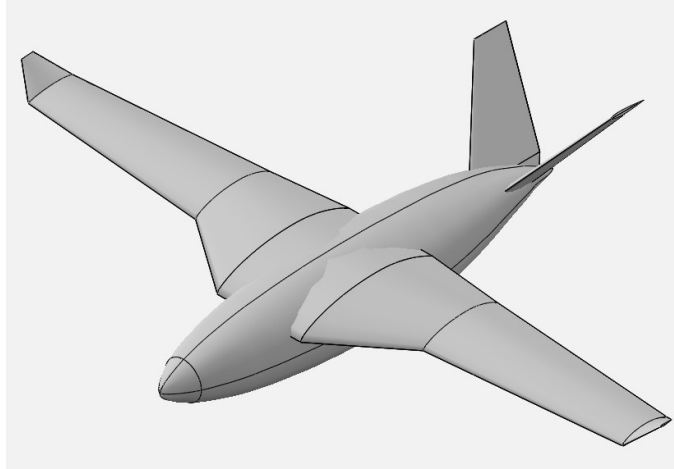
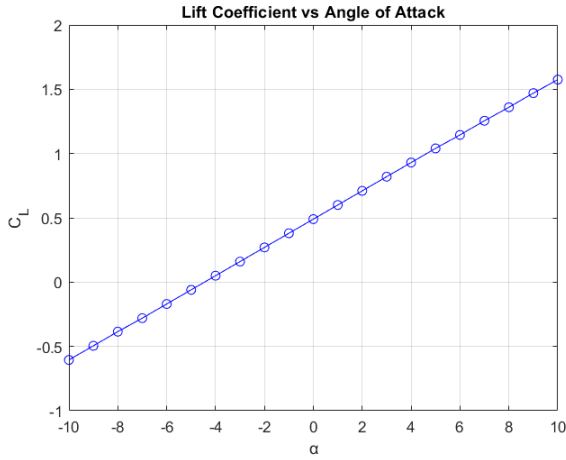
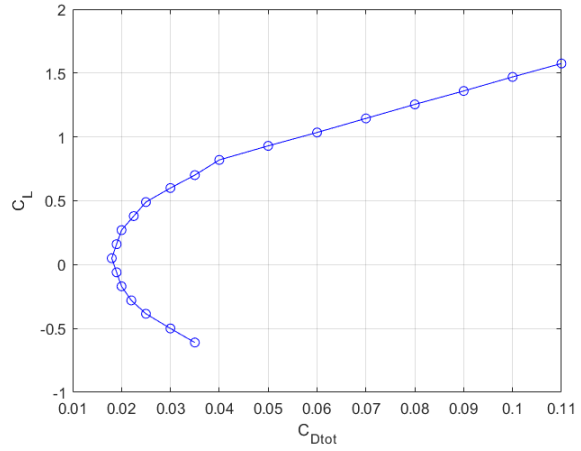
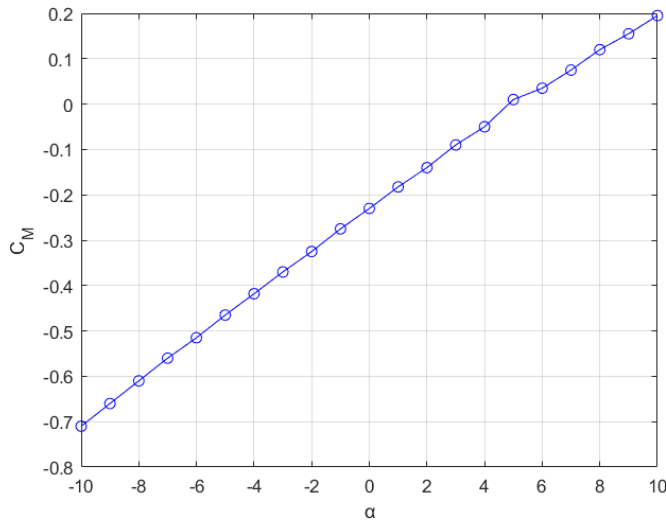


Figure 9: eVTOL concept for implementing FanFoil technology

4.2 External Aerodynamics Simulations

Low-fidelity aerodynamic coefficients were obtained using the OpenVSP model and running the Open VSPAERO feature for cruise conditions. An input speed of Mach 0.22 and a Reynolds number of 6.5×10^6 was used for the simulation. Figures 10, 11 and 12 show the lift coefficient vs angle of attack, the drag polar, and the pitching moment coefficient versus angle of attack respectively. Results show a linear lift-curve-slope with a value of $0.11/\text{deg}$ which is equivalent to the theoretical result for airfoils. VSPAERO does not model flow separation or the effect of wing aspect ratio, which is the rationale for the simplistic lift-curve-slope result. The drag polar is used to graphically find the base drag coefficient, $C_{D0} = 0.018$ and the lift-to-drag ratio, $L/D = 15.0$ which are reasonable values for a clean aircraft configuration at the cruise Reynolds number. With the wings attached to the fuselage at an angle of incidence of -4 degrees, the lift coefficient shows a value of $C_L = 0.5$ at $\alpha = 0^\circ$. The drag polar chart displays the so called "drag bucket" existing within the range of $C_L = -0.18$ to 0.29 . This results suggests that the wing area should increase in order to bring down the design lift coefficient from 0.45 to below 0.30 . The pitching moment coefficient graph displays that the aircraft will tend to have a "nose-down" pitching behavior in cruise conditions, which represents positive longitudinal static stability. The high pitching moment derivative, $dC_M/d\alpha$ is indicative of the high degree of airfoil camber, 7% of chord, which is not desired because this nose-down pitching moment must be compensated by considerably deflecting the V-tail control surfaces during cruise.

DOI: ADD DOINUMBER HERE

Figure 10: Lift coefficient, C_L vs angle of attack, α Figure 11: Drag polar, C_L vs C_D Figure 12: Pitching moment, C_M vs α

4.3 Full-Range Mission Analysis

A first-order analytical methodology is applied to determine eVTOL feasibility to complete a full-range mission, and then determine several flight routes between cities of interest in the state of Texas that the eVTOL can serve. Each mission is divided into a number of phases from which the analysis is simplified and can be carried out. The mission phases considered in sequential order during flight are as follows: (i) vertical takeoff, (ii) transition to forward flight, (iii) climb, (iv) cruise, (v) descent, (vi) transition to hover, and (vii) vertical landing. The analytical formulation is applied for each phase to determine power consumption and energy expenditure.

4.3.1 Vertical Takeoff

The ideal power for vertical takeoff is calculated for the large ducted fans on the inboard wing panels, and the regular fans on the wing flaps. First, the thrust for vertical takeoff is assumed as,

$$T_{VTO} = 1.2T_H \quad (4)$$

DOI: ADD DOINUMBER HERE

where the hover thrust is equal to the takeoff weight of the aircraft, $T_H = W_{T0}$. The ideal power for vertical takeoff using a number of ducted fans, n_F of fan disk area, A_F modified from momentum theory for an open propeller is then given as,

$$P_{i,VTO} = 0.5 \frac{T_{VTO}^{3/2}}{\sqrt{\rho n_F A_F}} \quad (5)$$

We can use this expression to solve for the ideal vertical takeoff power produced by each of the six large ducted fans, P_{LF} and 20 regular ducted fans, P_{RF} . Note that during takeoff, the large fans provide thrust equal to 45% of the takeoff weight, and the regular fans provide thrust equal to 75% of the takeoff weight. The ideal power per fan is thus,

$$\begin{aligned} P_{i,LF} &= 0.5 \frac{(0.375T_{VTO})^{3/2}}{\sqrt{6\rho A_{LF}}} \\ P_{i,RF} &= 0.5 \frac{(0.625T_{VTO})^{3/2}}{\sqrt{20\rho A_{RF}}} \end{aligned} \quad (6)$$

where the fan disk area of the large and regular ducted fans is 0.159 m^2 and 0.071 m^2 respectively, based on fan diameters of 0.45 m and 0.30 m .

The actual power produced by each fan is calculated by by dividing the ideal power by the product of the propulsion system efficiency, η_{Prop} and battery efficiency, η_B . The propulsion system considers a number of component efficiencies, η namely from the electric motor, η_M , duct, η_D , fan, η_F , and electric distribution, η_{e-dist} . The overall propulsion efficiency is given by the product of the component efficiencies,

$$\eta_{Prop} = \eta_M \cdot \eta_D \cdot \eta_F \cdot \eta_{e-dist} \quad (7)$$

The actual power consumption for each fan is then expressed as follows,

$$\begin{aligned} P_{a,LF} &= \frac{P_{i,LF}}{\eta_{Prop} \cdot \eta_B} \\ P_{a,RF} &= \frac{P_{i,RF}}{\eta_{Prop} \cdot \eta_B} \end{aligned} \quad (8)$$

The values for the propulsion component efficiencies and battery efficiency are given on Table 1. The total actual power and energy required for vertical takeoff is also given, assuming a short vertical takeoff time, t_{VTO} of 15 seconds,

$$E_{VTO} = [(P_{a,LF} \cdot n_{LF}) + (P_{a,RF} \cdot n_{RF})] \cdot t_{VTO} \quad (9)$$

Table 3: Vertical takeoff component efficiencies and performance

Component/ Performance	Efficiency, η	Electric Power, P_{elec}	VTO Energy, E_{VTO}
Motor	0.95		
Duct	0.94		
Fan	0.85		
Elec. Distribution	0.97		
Battery	0.85		
Overall System, $\eta_{Prop} \cdot \eta_B$	0.63		
Electric Power		2.23 GW	

VTO Energy

9.31kW-hr

4.3.2 Transition to Forward Flight

The transition to forward flight is a relatively complex flight maneuver that involves time-dependent thrust vectoring of the propulsion fans and lift produced by the main wing due to forward flight. The longitudinal stability must also be maintained by adjusting power and thrust between the large fans in front of the center of gravity, and the regular fans on the flaps of the wing behind the CG. In terms of the fan power consumption, we can assume an average actual transition power using the hover power (beginning of transition) and the power at the end of transition. This is defined as when the aircraft reaches its stall speed and the fans have fully rotated providing complete forward thrust. The end of transition power is estimated as 10% of the actual hover power, thus the average transition power simplifies to,

$$P_{Tr,avg} = 0.55P_H \quad (10)$$

where the actual transition power is calculated as 1.23 GW. The stall speed of the eVTOL is estimated by replacing the operating lift coefficient, C_L with the maximum lift coefficient, $C_{L,max}$ of the wing-body geometry. This is approximated from a NACA report for a clean wing-body geometry with an aspect ratio, A of 8.09 and a wing taper ratio, λ of 0.5. The configuration is operating at a mean Reynolds number, Re of 5.1×10^6 . The $C_{L,max}$ is stated as 1.33. In terms of aspect and taper ratio, as well as Re near the stall speed, the wing-body geometry is comparable to the eVTOL and thus we assume a $C_{L,max}$ of 1.33 to calculate the stall speed of 36.62 m/s (132 km/h) using the expression below,

$$V_{St} = \sqrt{\frac{2L}{\rho S C_{L,max}}} \quad (11)$$

The next step to calculating the transition time is to assume that the aircraft travels forward with an average acceleration, a_{Tr} of $0.20g$ (1.96 m/s^2) which is a reasonable assumption. The transition time is then calculated as,

$$t_{Tr} = \frac{V_{St}}{a_{Tr}} \quad (12)$$

which is computed as $t_{Tr} = 18.7$ sec. The energy consumption can now be calculated using the equation,

$$E_{Tr} = P_{Tr,avg} \cdot t_{Tr} \quad (13)$$

The transition energy is calculated as 6.38 kW-hr. A summary of the transition phase variables are shown on Table 4.

Table 4: Transition to forward flight component efficiencies and performance

Component/ Performance	Efficiency, η	Electric Power, P_{elec}	Transition Energy, E_T
Motor	0.95		
Duct	0.94		
Fan	0.85		
Elec. Distribution	0.97		
Battery	0.85		
Overall System, $\eta_{prop} \cdot \eta_B$	0.63		
Electric Power		1.23 GW	
Transition Energy			6.38kW-hr

4.3.3 Climb

At the end of transition to forward flight, the aircraft accelerates from a stall speed of 132 km/hr to the climb velocity, $V_{cl} = 196$ km/hr before initiating a climb maneuver at a climb angle, $\Phi = 12^\circ$. The climb power can be approximated by considering the climb drag and the aircraft weight component in the direction of flight, as well as the climb velocity. It

DOI: ADD DOINUMBER HERE

will be assumed, for simplification, that the airframe component drag, D_i for the wing, fuselage, and tail in climb are equivalent to that in cruise. The climb power is thus expressed as,

$$P_{Cl} = \frac{\sum_i D_i + W_{TO} \cdot \sin(\Phi) \cdot V_{Cl}}{\eta_{Prop} \cdot \eta_P \cdot \eta_B} \quad (14)$$

where the additional propulsive efficiency term, η_P is added to represent the loss in power from the ducted fan jet to the power delivered to the aircraft. This is approximated as $\eta_P = 0.87$ for climb using the Froude equation and a momentum analysis approach. The climb power is then calculated as 990 kW. The time to climb can be estimated by considering the cruise altitude, H of 8,000 ft (2,439 m) and the vertical climb rate using the climb velocity and angle as follows,

$$t_{Cl} = \frac{H}{V_{Cl} \cdot \sin(\Phi)} \quad (15)$$

The time to climb is approximated as 3.6 minutes. The climb energy is now calculated as the product of the two equations above,

$$E_{cl} = P_{cl} \cdot t_{cl} \quad (16)$$

where the energy required for climb is estimated as 59.28 kW-hr. During the climb phase, the eVTOL travels a horizontal distance equal to 11.47 km which is added to the total range of the aircraft. A summary of the climb variables and performance is given on Table 5.

Table 5: Climb component efficiencies and performance

Component/ Performance	Efficiency, η	Electric Power, P_{elec}	Climb Energy, E_c
Motor	0.95		
Duct	0.94		
Fan	0.85		
Elec. Distribution	0.97		
Battery	0.85		
Propulsive Efficiency	0.87		
Overall System, $\eta_{Prop} \cdot \eta_B$	0.63		
Electric Power		990 kW	
Climb Energy			59.28 kW-hr

4.3.4 Cruise

The majority of the full-range mission is spent in the cruise phase, where the eVTOL is in steady unaccelerated flight at the cruise altitude. We will assume that the aircraft reaches cruise conditions, including cruise Mach number of 0.22, immediately after climb. The first step in the cruise analysis is to estimate the total aircraft drag in cruise, which is the sum of the component drag terms; wing, D_W , fuselage, D_F , and tail, D_T ,

$$D_{Tot} = \sum_i D_i = D_W + D_F + D_T \quad (17)$$

The component drags are calculated using first-order analytical formulation as outlined in aircraft design texts. For brevity in the analysis, the formulation and discussion will be limited to drag calculations. The main wing operates at a Reynolds number of 6.97×10^6 based on mean aerodynamic chord, Re_{mac} . The skin friction coefficient, C_f is based on turbulent flow on a flat plate and also the cruise Mach number, where $C_f = 0.0032$. The wing form factor, F is approximated as a function of the location of the airfoil's maximum thickness, x/c , maximum airfoil thickness-to-chord ratio, t/c , the Mach number, and the wing sweep angle at maximum thickness. The form factor was estimated as $F = 1.23$. An interference factor, Q , accounting for interference drag between the wing and ducted fans mounted on the underside of the wing was estimated as 1.2. Finally, a wing efficiency factor, e , of 0.85 was used. The base drag coefficient for the wing was found to be 0.009526

DOI: ADD DOINUMBER HERE

and total wing drag coefficient, including base and induced drag, was found using the equation below,

$$C_D = \frac{C_f \cdot FF \cdot Q \cdot S_{wet}}{S_{ref}} + \frac{1}{\pi A e} \cdot C_L^2 \quad (18)$$

The total wing drag coefficient is 0.0172 for a lift-to-drag ratio of 24.97, reasonable for a clean wing design. The total drag is now obtained from the drag equation,

$$D_W = \frac{1}{2} \rho V_\infty^2 S C_D \quad (19)$$

A similar drag analysis was conducted for both the fuselage and tail, using relevant parameters and calculations for these components. A summary of the drag calculations are shown on Table 6.

Table 6: Drag Estimates [N]

	Wing	Fuselage	Tail
Drag Component, D_o	994.6	374.5	215.9
Total drag, D_{TOT}	1585		

In cruise thrust equals the total drag, so the flight power consumption in cruise can be calculated readily. The actual power in cruise considering system efficiencies can be calculated using the expression,

$$P_{Cr} = \frac{D_{TOT} \cdot V_{Cr}}{\eta_{Prop} \cdot \eta_P \cdot \eta_B} + 10kW \quad (20)$$

Given a cruise time of 0.93 hours, the total cruise energy requirement can be calculated,

$$E_{cr} = P_{cr} \cdot t_{cr} \quad (26)$$

System efficiencies from previous phases remain unchanged except battery efficiency increases to 0.98 in cruise. Ten kW of power is added to that required for propulsion to account for auxiliary power to other flight systems.

Table 7: Cruise component efficiencies and performance

Component/ Performance	Efficiency, η	Electric Power, P_{elec}	Cruise Energy, E_{VTO}
Motor	0.95		
Duct	0.94		
Fan	0.85		
Elec. Distribution	0.97		
Battery (in cruise)	0.98		
Propulsive Efficiency	0.87		
Overall System, $\eta_{prop} \cdot \eta_B$	0.63		
Electric Power		178.7 kW	
Cruise Energy			166.4 kW-hr

From the above analysis of each flight phase, the total energy required for a maximum-range mission may be determined by summing the energy requirements of each individual phase. The results are presented on Table 8. It was determined that the total energy required for the mission is 260.47 kW-h, and with a 3% battery energy reserve, a total of 268.28 kW-h is required which is just below the available energy from the battery of 270 kW-h.

DOI: ADD DOINUMBER HERE

Table 8 Total Aircraft Energy Consumption

Phase	Duration, sec (hr)	Horizontal Distance Traveled, km (mi)	Energy Required, kW-h
Vertical takeoff	15.0 (0.004)	0 (0)	9.31
Transition to forward flight	18.7 (0.005)	0.340 (0.21)	6.38
Climb	216 (0.06)	12.68 (7.87)	59.05
Cruise	3352 (0.93)	261.74 (162.6)	166.45
Descent	600 (0.167)	35.96 (22.3)	4.96
Transition to hover	18.7 (0.005)	0.340 (0.21)	6.38
Vertical landing	15.0 (0.004)	0 (0)	7.91
Subtotal	4508 (1.252)	311.06 (193.2)	260.47
3% Reserve	N/A	N/A	7.79
Total	4508 (1.252)	311.06 (193.2)	268.28

This data is invaluable in determining concept feasibility. The intended application is short, inter-city commutes that are significantly affected by road congestion or other traffic limitations. Three common and relevant routes in the state of Texas were identified as feasible to travel to given the maximum range of the eVTOL which is calculated as 193 miles. **1. Waco to DFW:** Distance of 110 miles and average car commute of 1 hour and 45 minutes. Commute time would be reduced by a full hour to \approx 45 minutes with this eVTOL design. **2. San Antonio to Austin:** Distance of 80 miles and average car commute of 1 hour and 40 minutes (long commute time due to heavy traffic on the I-35 corridor). Commute time would be reduced to \approx 30 minutes or about 1/3 of the time with this eVTOL design. **3. Austin to Houston:** Distance of 162 miles and average car commute of 2 hours and 47 minutes. Commute time would be reduced to \approx just over 1 hour with this eVTOL design.

5. Conclusions

This paper presents the conceptual design for a revolutionary eVTOL concept that uses the ‘FanFoil’ technique introduced in this paper. Computational ANSYS simulations are presented for the new Maldonado-Hicks airfoil at the cruise conditions of the eVTOL aircraft. OpenVSP was used to model the 3D geometry of the aircraft. While the VSPAERO aerodynamic results do not consider flow three-dimensionality or flow separation, they are encouraging as a preliminary tool to evaluate the base drag coefficient aerodynamic efficiency of the aircraft in cruise. Future work is directed in three areas: (i) Tuning the geometric properties (including curvature and camber) of the Maldonado-Hicks airfoil in order to improve max L/D and/or shift the L/D point to a lower angle of attack closer to the cruise angle of attack. (ii) 3D model a wing section without and with an array of ducted fans mounted below the wing and run ANSYS simulations to assess the aerodynamic impact of the fans. The accuracy of unsteady rotor flows are difficult to predict using CFD, therefore (iii) a wind tunnel study of the eVTOL using a 1/8th scale half-body model will be carried out. The model will contain removable ducted fans in order to measure their effect on lift, drag, pitching moment, and ultimately determine the aerodynamic merit of the underwing mounting fan technique. Other experiments to measure the thrust and power required in forward flight will be conducted in order to obtain more accurate energy calculations to update the mission analysis and feasible mission.

References

- [1] Kadhiresan, A.R., and Duffy, M.J. 2019. Conceptual design and mission analysis for eVTOL urban air mobility flight vehicle Configurations. *AIAA Aviation Conference*, AIAA, Washington, DC.
- [2] Ha, T.H., Lee, K., and Hwang, J.T. 2019. Large-scale design-economics optimization of eVTOL concepts for urban air mobility. *AIAA SciTech Conference*, AIAA, Washington, DC, 2019.

DOI: ADD DOINUMBER HERE

- [3] Joby Aviation. URL <https://jobyaviation.com/>, [Accessed: November 2022].
- [4] Archer Aviation. URL <https://archer.com/>, [Accessed: November 2022].
- [5] Lilium. URL <https://lilium.com/>, [Accessed: November 2022].
- [6] Boundary Layer Ingestion Propulsion - Glenn Research Center. URL <https://www1.grc.nasa.gov/aeronautics/bli/>, [Accessed: November 2022].
- [7] Uranga, A., and et al. 2018. Analysis of the aerodynamic benefit from boundary layer ingestion for transport aircraft. *AIAA Journal*. <https://doi.org/10.2514/1.j056781>.
- [8] Ayele, W., McEntire, C., Green, L., Prakash, B., Farley-Talamantes, E., and Maldonado, V. 2022. Conceptual design of a robotic ground-aerial vehicle for mars planetary exploration. *AIAA Aviation Conference*, AIAA, Chicago, IL.
- [9] Santos, D., Ramirez, D., Rogers, J., Zamora, J., Rezende, A., and Maldonado, V. 2022. Full-cycle design and analysis of the switchblade reconfigurable unmanned aerial system. *AIAA Aviation Conference*, AIAA, Chicago, IL.
- [10] Wilt, M., Hicks, J., Saleem, W., M., B., R., T., Waszkowskly, Reynolds, C., Selvey, J., Ritchie, C., Shapiro, N., and Maldonado, V. 2022. Conceptual design of a multi-flight regime reconfigurable combat aerial vehicle,” *AIAA Aviation Conference*, AIAA, Chicago, IL.
- [11] Raymer, D., *Aircraft Design: A Conceptual Approach*, 5th ed., American Institute of Aeronautics and Astronautics, Reston, VA, 2012.
- [12] Gundlach, J., *Designing Unmanned Aircraft Systems: A Comprehensive Approach*, American Institute of Aeronautics and Astronautics, Reston, VA, 2012.

DOI: ADD DOINUMBER HERE

DOI: ADD DOINUMBER HERE

References

- 4.3.1.1 Kadhiresan, A. R., and Duffy, M. J., “Conceptual Design and Mission Analysis for eVTOL Urban Air Mobility Flight Vehicle Configurations,” *AIAA Aviation Conference*, AIAA, Washington, DC, 2019.
- 4.3.1.2 Ha, T. H., Lee, K., and Hwang, J. T., “Large-scale Design-economics Optimization of eVTOL Concepts for Urban Air Mobility,” *AIAA SciTech Conference*, AIAA, Washington, DC, 2019.
- 4.3.1.3 “Joby Aviation,” , ??? URL <https://jobyaviation.com/>, [Accessed: November 2022].
- 4.3.1.4 “Archer Aviation,” , ??? URL <https://archer.com/>, [Accessed: November 2022].
- 4.3.1.5 “Lilium,” , ??? URL <https://lilium.com/>, [Accessed: November 2022].
- 4.3.1.6 “Boundary Layer Ingestion Propulsion - Glenn Research Center,” , ??? URL <https://www1.grc.nasa.gov/aeronautics/bli/>, [Accessed: November 2022].
- 4.3.1.7 Uranga, A., and et al., “Analysis of the Aerodynamic Benefit from Boundary Layer Ingestion for Transport Aircraft,” *AIAA Journal*, Sept 2018. <https://doi.org/10.2514/1.j056781>.
- 4.3.1.8 Ayele, W., McEntire, C., Green, L., Prakash, B., Farley-Talamantes, E., and Maldonado, V., “Conceptual Design of a Robotic Ground-Aerial Vehicle for Mars Planetary Exploration,” *AIAA Aviation Conference*, AIAA, Washington, DC, 2022.
- 4.3.1.9 Santos, D., Ramirez, D., Rogers, J., Zamora, J., Rezende, A., and Maldonado, V., “Full-Cycle Design and Analysis of the Switchblade Reconfigurable Unmanned Aerial System,” *AIAA Aviation Conference*, AIAA, Washington, DC, 2022.
- 4.3.1.10 Wilt, M., Hicks, J., Saleem, W., M., B., R., T., Waszkowsky, Reynolds, C., Selvey, J., Ritchie, C., Shapiro, N., and Maldonado, V., “Conceptual Design of a Multi-Flight Regime Reconfigurable Combat Aerial Vehicle,” *AIAA Aviation Conference*, AIAA, Washington, DC, 2022.
- 4.3.1.11 Raymer, D., *Aircraft Design: A Conceptual Approach*, 5th ed., American Institute of Aeronautics and Astronautics, Reston, VA, 2012, pp. 223 – 225. <https://doi.org/10.2514/4.869112>.
- 4.3.1.12 Gundlach, J., *Designing Unmanned Aircraft Systems: A Comprehensive Approach*, American Institute of Aeronautics and Astronautics, Reston, VA, 2012.